*remote sensing*

*Article*

# Dynamic Analysis of Regional Wheat Stripe Rust Environmental Suitability in China

**Linsheng Huang [1], Xinyu Chen [1], Yingying Dong [2,*], Wenjiang Huang [2,3], Huiqin Ma [2], Hansu Zhang [1], Yunlei Xu [1] and Jing Wang [1]**

[1] National Engineering Research Center for Agro-Ecological Big Data Analysis and Application, Anhui University, Hefei 230601, China
[2] State Key Laboratory of Remote Sensing Science, Aerospace Information Research Institute, Chinese Academy of Sciences, Beijing 100094, China
[3] University of Chinese Academy of Sciences, Beijing 100049, China
* Correspondence: dongyy@aircas.ac.cn

**Abstract:** Stripe rust is one of the most destructive wheat diseases in China, negatively affecting the production safety and causing yield losses of wheat. Thus, it is important to analyze the environmental suitability and dynamic changes of wheat stripe rust in China. The occurrence of stripe rust is affected by multiple factors. Therefore, this study combined data from various disciplinary fields such as remote sensing, meteorology, biology, and plant protection to evaluate the environmental suitability of stripe rust in China using species distribution models. The study also discusses the importance and effect of various variables. Results revealed that meteorological factors had the greatest impact on the occurrence of stripe rust, especially temperature and precipitation. Wheat growth factors have a greater impact from April to August. Elevation has a greater impact in summer. The ensemble model results were better than the single model, with TSS and AUC greater than 0.851 and 0.971, respectively. Overlapping analysis showed that the winter stripe rust suitable areas were mainly in the Sichuan Basin, Northwestern Hubei, Southern Shaanxi, and Southern Henan wheat areas. In spring, the suitable areas of stripe rust increased in Huang-Huai-Hai and the middle and lower reaches of the Yangtze River and Guanzhong Plain, and the development of northwestern wheat areas such as Xinjiang and Gansu slightly lagged behind. In summer, wheat threatened by stripe rust is mainly in late-ripening spring wheat areas in Gansu, Ningxia, Qinghai, and Xinjiang. This study can provide a scientific basis for optimizing and improving the comprehensive management strategy of stripe rust.

**Keywords:** wheat; stripe rust; suitable areas; species distribution models

check for updates

**Citation:** Huang, L.; Chen, X.; Dong, Y.; Huang, W.; Ma, H.; Zhang, H.; Xu, Y.; Wang, J. Dynamic Analysis of Regional Wheat Stripe Rust Environmental Suitability in China. *Remote Sens.* **2023**, *15*, 2021. https://doi.org/10.3390/rs15082021

Academic Editor: Jochem Verrelst

Received: 12 February 2023
Revised: 28 March 2023
Accepted: 7 April 2023
Published: 11 April 2023



## 1. Introduction

Wheat stripe rust, caused by *Puccinia striiformis* f. sp. *tritici* (Pst), is one of the diseases that negatively affect the safety of wheat production [1]. China is the largest independent endemic area of stripe rust in the world. More than 20 million hectares of wheat are affected by stripe rust, and wheat yield can be reduced by more than 40% in epidemic years [2]. Therefore, studying the areas with environmental conditions suitable for stripe rust development and their dynamic changes in China is of great significance. Species distribution models (SDMs) are widely used to predict species invasion and the potential distribution of endangered species and analyze the impact of climate change on the potential distribution of species [3]. There are also many studies on the distribution of harmful species in agriculture [4]. Many studies have used SDMs to study the distribution of crop diseases, such as maize downy mildew [5], wheat blast, and stripe rust [6,7]. Therefore, applying SDMs for the environmental suitability analysis of wheat stripe rust can help predict its occurrence and epidemic, implement comprehensive prevention and control measures, and ensure the safety of grain production.

Pst can disperse long distance by wind movement and human-assisted transport and requires susceptible host plants (mainly wheat) to survive and reproduce [8]. Stripe rust is a low-temperature disease that does not oversummer in most wheat-growing regions [9]. In China, stripe rust can oversummer on volunteer wheat seedlings in the mountainous regions of Southern Gansu, Eastern Qinghai, Northwestern Sichuan, and Southern Ningxia [10]. In summer, the maximum temperature in the oversummering areas is always lower than 22 °C, and sufficient precipitation creates favorable environmental conditions for the reproduction of the pathogen [11]. Pst migrates to low elevation to infect autumn seedlings and disperse southward and eastward via air currents, infecting autumn seedlings and overwintering in the Sichuan Basin, Yunnan, Guizhou, Western Hubei and Southern Henan [10,12]. The temperature difference between the north and south is huge in winter, with the Qinling–Huaihe Line (the 0 °C isotherm) serving as the dividing line, and the highest temperature in the south can reach above 20 °C [13]. Spores can reproduce continuously on wheat due to relatively warm temperatures or survive in the form of mycelium in wheat leaves at low temperature in these regions [11,14]. In the spring of the following year, spores are dispersed toward the northeast into the main wheat production areas, including Henan, Shandong, Hebei, and other provinces [11,12].

Apart from suitable host plants and sufficient inoculum sources, environmental conditions are also important factors affecting stripe rust epidemics. Available evidence suggests that the infection and development of stripe rust is very temperature dependent, and the optimal temperature required for its growth is 10–15 °C [15,16]. However, Vidal et al. [17] showed that the different Pst pathotypes do not respond in the same way to temperatures. Suitable precipitation and humidity provide favorable conditions for the infection and reproduction of the pathogen [18]. The prediction model established by Guo et al. [19] showed that average temperature and relative humidity were the determinants of the occurrence of stripe rust in the Sichuan Basin. The study by Naseri et al. [20] showed that air temperature, icy and rainy days, relative humidity, and region over an autumn, winter, and spring period had a combined effect on the stripe rust epidemics in Kermanshah, Iran. Moreover, other environmental factors such as sunshine, wind, snow cover, and geographical factors such as elevation can affect the occurrence of stripe rust [21–23]. Yang et al. [24] used four meteorological variables, namely temperature, humidity, precipitation, and sunshine hours, to establish a prediction model, and the results could well reflect distribution and spatiotemporal development of stripe rust in Gansu.

With the changes in climate and farming systems and the development of new wheat varieties, the suitable area of wheat stripe rust may change, so it is necessary to improve existing research. In the past, large-scale studies of wheat stripe rust were usually based on meteorological factors and empirical knowledge obtained from extensive field investigations and analyzed through methods such as threshold setting [16,20,25]. At the same time, these studies also suggest that studying the regional epidemic of stripe rust based only on one or more meteorological factors may lead to deviations from the reality, and there is still room for improvement. Therefore, it is necessary to consider the growth status of wheat, such as the planting distribution, growth period, and vegetation condition of wheat [26]. Furthermore, factors such as topography and soil often influence the distribution of species on smaller spatial scales [27]. The use of remote sensing data, which can provide a time series of information on vegetation status, productivity, and seasonal changes, has been shown to improve model performance and transferability as well as improve the possibility of simulating the distribution of species over time, making the results more reasonable [28].

This study is based on the development and epidemic patterns of wheat stripe rust. Using downscaled meteorological data, elevation data, and spectral data provided by remote sensing, taking into account wheat distribution, ensemble SDMs were used to assess the environmental suitability of wheat stripe rust. The main goals in this study were: (1) to select environmental factors affecting the occurrence of wheat stripe rust, build a model for extracting monthly wheat stripe rust suitable areas, and map the suitable areas for stripe rust in China and (2) to analyze the importance of environmental variables in the model for each month and explore the impact of multiple variables on the distribution of stripe rust suitable areas in major stripe rust ecological zones in China.

## 2. Materials and Methods

### *2.1. Study Area*

Located in the east of Asia and on the west coast of the Pacific Ocean, China covers a total area of 9.6 million square kilometers, and the elevation is high in the west and low in the east [29]. The complex climatic conditions and wheat-planting system provide environmental conditions for the occurrence and annual cycle of stripe rust. Most areas belong to the monsoon climate type, with abundant rainfall in summer, a long rainy season in the south, and short rainy season in the north while being relatively dry in winter [11]. The temperature difference between the north and south is huge in winter, with the Qinling–Huaihe Line (the 0 °C isotherm) serving as the dividing line, where the highest temperature in the south can reach above 20 °C, and the lowest temperature in the north can drop to −30 °C [13,29]. In summer, with the exception of high-altitude areas such as the Qinghai–Tibet Plateau, most regions have temperatures above 20 °C [13]. Wheat is planted all over China, and more than 75% of wheat-planting areas are planted using a multi-cropping system [30].

### *2.2. Data*

#### 2.2.1. Occurrence Records and Wheat Distribution Data

The occurrence record of wheat stripe rust from 2009 to 2014 came from the Agricultural Technology Center, which recorded the occurrence of stripe rust in the wheat growth period in counties across the country. To reduce the spatial correlation, SDM toolbox v2.5 was used to spatially rarefy the data with a minimum radius of 10 km, so that occurrence localities can be reduced to a single point within the specified distance [31].

In order to obtain more precise coordinates of stripe rust, further study was conducted using wheat distribution data. The wheat distribution data were obtained from the ChinaCropArea 1 km dataset [32], which provides a 1 km-grid crop phenological dataset for wheat in China, including three phenological periods. Combined with the relevant research, the distribution of wheat and the time of planting and maturity were processed [33]. In Figure 1, northern winter wheat is distributed in the south of the Great Wall, east of the Liupan Mountains and Qinling Mountains (zones I and II). Southern winter wheat is distributed in the south of the Huaihe River and Qinling Mountains (zones III, IV, and V). Spring wheat is distributed in the north of the Yangtze River and Minshan Mountains (zones VI, VII, and VIII). Xinjiang and Qinghai–Tibet plant both winter wheat and spring wheat (zones IX and X). The results are shown in Figure 2.

#### 2.2.2. Environmental Data

The environmental variables used in this study include meteorological, vegetation, and elevation data. Meteorological data include mean minimum temperature (TMN), mean temperature (TMP), mean maximum temperature (TMX), precipitation (PRE), precipitation days (PD), relative humidity (RHU), and sunshine duration (SSD). Remote sensing data include enhanced vegetation index (EVI), leaf area index (LAI) and fractional vegetation coverage (FVC). All the above variables except elevation are the average monthly data from January to August (2010–2014) and December of the previous year (2009–2013).

TMN, TMP, TMX, and PRE were downloaded from the National Tibetan Plateau Data Center. The datasets were generated by downscaling through the Delta spatial downscaling scheme according to the global 0.5° climate dataset published by CRU and the global high-resolution climate dataset published by WorldClim. The data format is NETCDF, and the spatial resolution is 0.0083333° (about 1 km) [34].

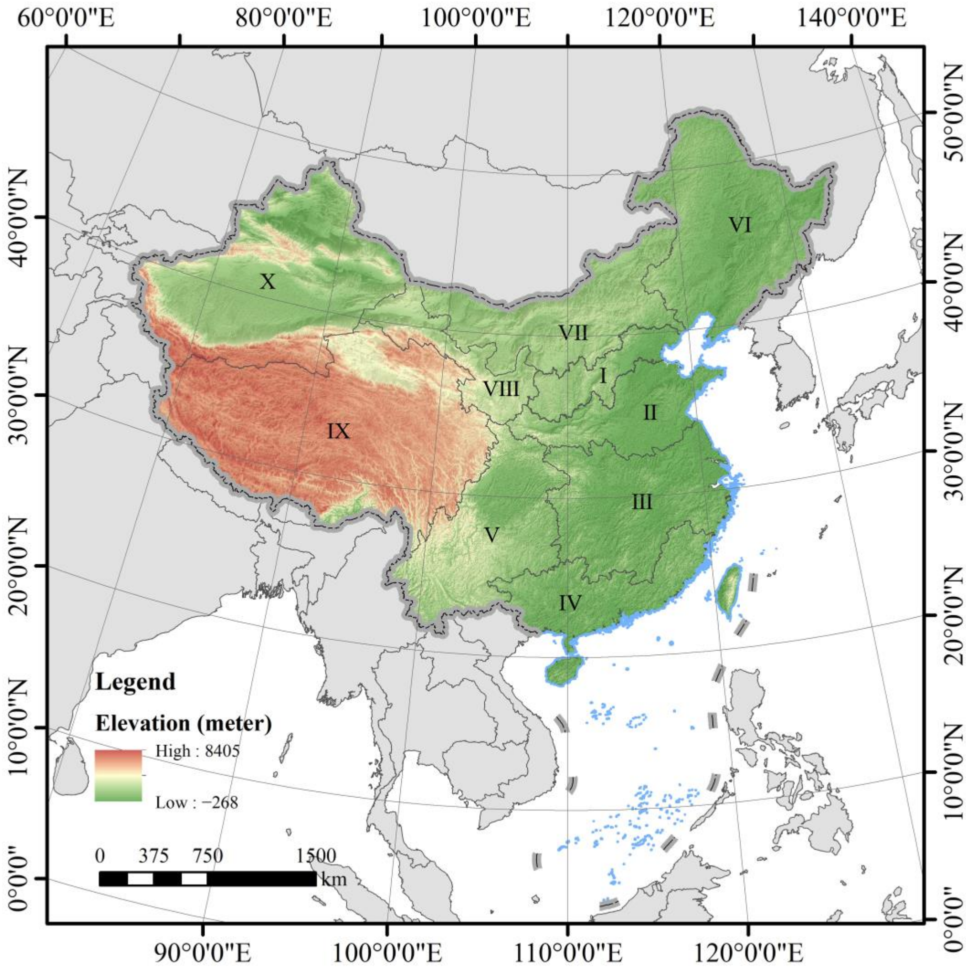


**Figure 1.** The geographical location of the study area. Major agro-ecological zones of wheat in China are indicated by Roman numerals [30]. Adapted with permission from Ref. [30]. 2009, Elsevier. The Digital Elevation Model (DEM) of China is available from the Resource and Environmental Science and Data Center.

RHU and SSD are obtained from National Earth System Science Data Center, National Science and Technology Infrastructure of China. The data are based on the monthly relative humidity and sunshine duration data of 824 ground meteorological stations in China. The 1 km-resolution DEM was used as a covariate to generate monthly raster data by spatial interpolation, and the interpolation used the thin plate spline method [35].

LAI and FVC data were derived from the Global Land Surface Satellite (GLASS) product, V60. The product is a long-term, high-precision global surface remote sensing product based on the inversion of multi-source remote sensing data and ground measured data. The spatial resolutions of LAI and FVC data are 1 km and 500 m, respectively, and the time resolution is 8 days [36].

PD was calculated using total precipitation from the ERA5-Land Hourly reanalysis dataset produced by ECMWF's Copernicus Climate Change Service (C3S). The spatial resolution of the product is 0.1 radians (about 10 km) [37]. The sum of the days with daily total precipitation greater than 0.1 mm is taken as the number of precipitation days per month. PD was calculated on the Google Earth Engine (GEE) platform.

EVI was calculated using MOD09GA V6.1 products provided by the Moderate-resolution Imaging Spectroradiometer (MODIS) on the Terra satellite. The spatial resolution is 500 m, and the temporal resolution is 1 day [38]. EVI was downloaded on the GEE platform.

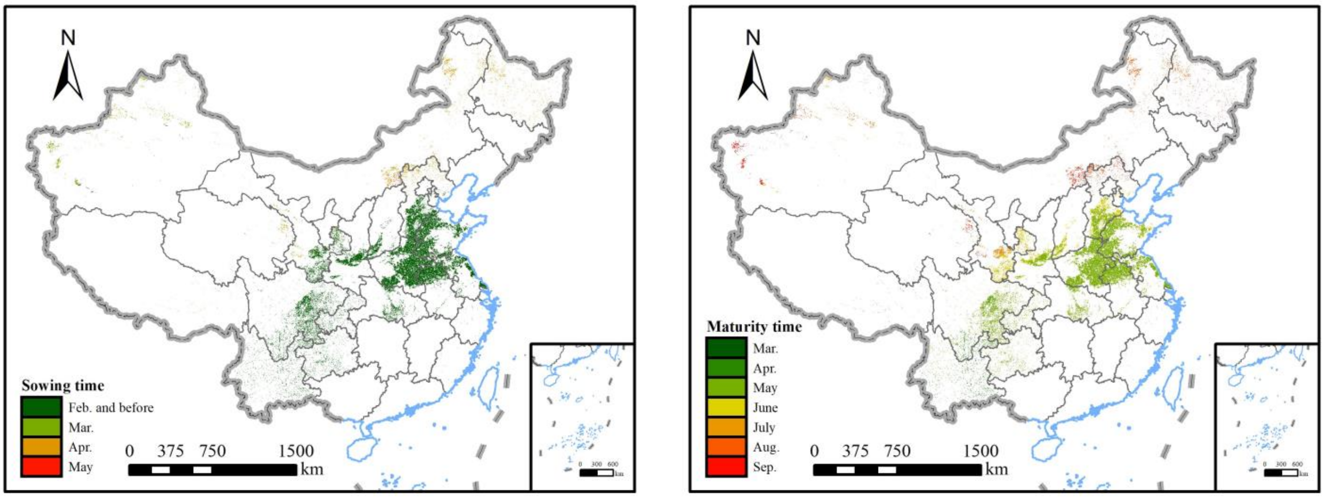


(**a**) Sowing time (**b**) Maturity time

**Figure 2.** The month of sowing and maturity of wheat in China from 2010 to 2014; (**a**) sowing time; (**b**) maturity time.

Elevation data obtained using the 90 m SRTM DEM were downloaded from the Resource and Environmental Science and Data Center, Chinese Academy of Sciences.

The data used in the study are all published raster data with a resolution of 1 km or resampled to 1 km using ArcGIS 10.6 software.

### *2.3. Variable Selection*

In order to avoid strong collinearity between variables, we calculated the Pearson's correlation coefficient between the variables and retained the variables with correlation <0.9 [39,40]. The variable with the highest Gini importance was selected among all strongly correlated variables by calculating the Gini importance of all candidate variables. The Gini importance was obtained by taking the average of the Gini impurity of each decision tree in the random forest and normalizing them. The formula for calculating the Gini importance is as follows:

$$s = norm\left(\frac{1}{k}\sum_{i}^{k} s_i\right) \quad (1)$$

where $s_i$ represent the Gini impurity of the $i$-th decision tree for each variable. The results of correlation analysis and Gini importance of variables are shown in Figure 3 and Table 1.

**Table 1.** The Gini importance of variables for each month.

| Variable | December | January | February | March | April | May | June | July | August |
|---|---|---|---|---|---|---|---|---|---|
| DEM | 0.117 | 0.107 | 0.027 | 0.061 | 0.044 | 0.054 | 0.227 | 0.130 | 0.074 |
| EVI | 0.018 | 0.025 | 0.011 | 0.018 | 0.335 | 0.179 | 0.161 | 0.109 | 0.144 |
| TMP | 0.107 | 0.124 | 0.173 | 0.143 | 0.092 | 0.085 | 0.034 | 0.027 | 0.012 |
| TMN | 0.193 | 0.137 | 0.188 | 0.273 | 0.049 | 0.064 | 0.017 | 0.026 | 0.013 |
| TMX | 0.047 | 0.123 | 0.177 | 0.044 | 0.034 | 0.075 | 0.019 | 0.079 | 0.022 |
| PRE | 0.218 | 0.225 | 0.218 | 0.196 | 0.142 | 0.128 | 0.331 | 0.286 | 0.304 |
| PD | 0.065 | 0.088 | 0.038 | 0.057 | 0.046 | 0.015 | 0.013 | 0.018 | 0.011 |
| RHU | 0.152 | 0.055 | 0.046 | 0.029 | 0.051 | 0.029 | 0.049 | 0.056 | 0.176 |
| SSD | 0.017 | 0.049 | 0.063 | 0.097 | 0.052 | 0.247 | 0.084 | 0.193 | 0.122 |
| FVC | 0.028 | 0.032 | 0.020 | 0.030 | 0.076 | 0.057 | 0.021 | 0.030 | 0.034 |
| LAI | 0.037 | 0.036 | 0.038 | 0.051 | 0.080 | 0.067 | 0.043 | 0.046 | 0.087 |

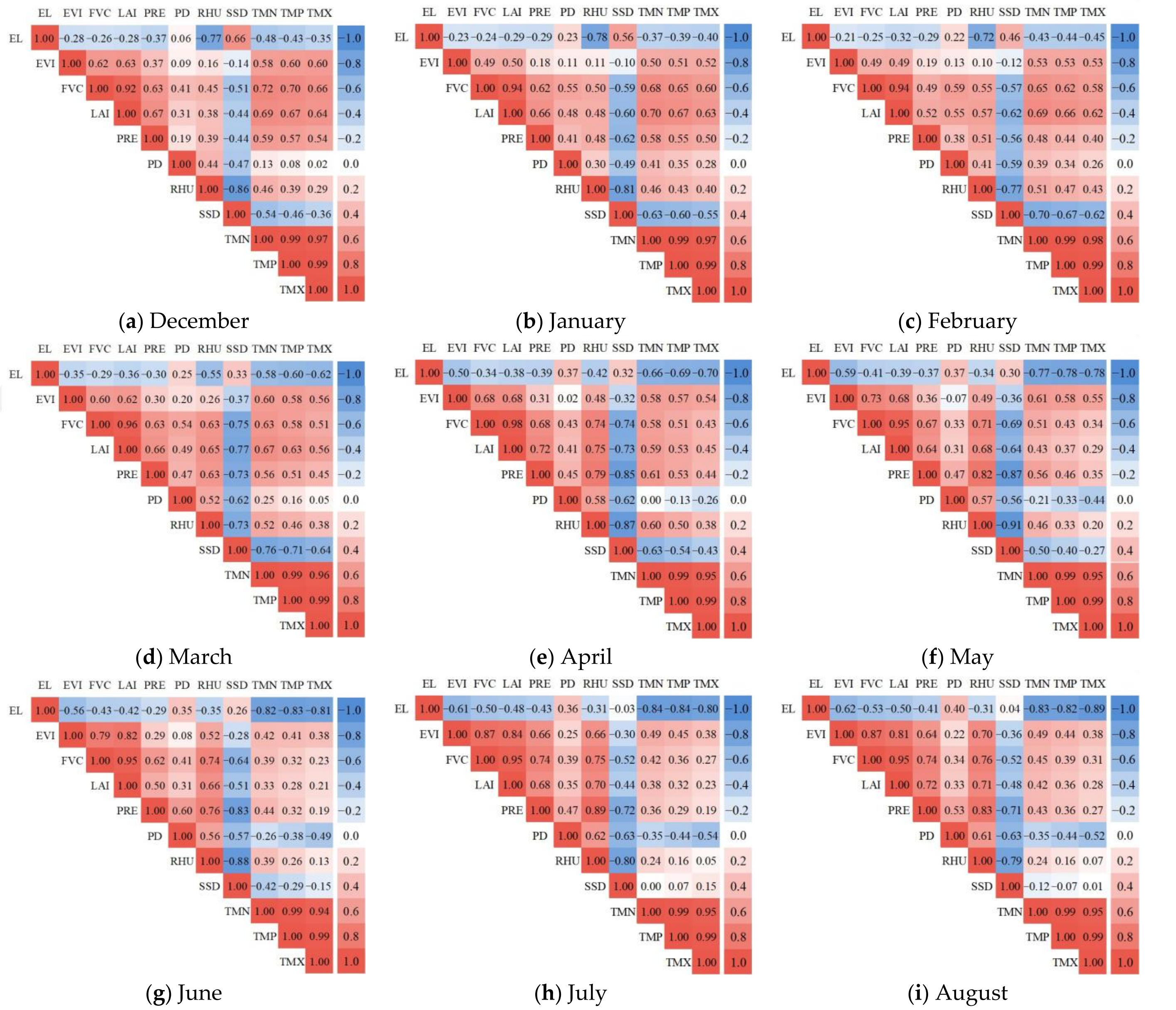


**Figure 3.** Pearson's correlation coefficient results for each month of variables from December to August. (**a**): The monthly variables are the five-year average values of the month from 2009 to 2013. (**b**–**i**): The monthly variables are the five-year average values of the month from 2010 to 2014.

The final variables used for modeling are shown in Table 2. From December to March, TMN has the largest weight among the three temperature variables, TMP has the largest weight from April to June, and TMX has the largest weight from July to August, so different temperature variables were selected in different months.

**Table 2.** List of the variables used for modeling.

| Month | Variable |
|---|---|
| December–March | TMN, PRE, PD, RHU, SSD, EVI, LAI, Elevation |
| April–June | TMP, PRE, PD, RHU, SSD, EVI, LAI, Elevation |
| July, August | TMX, PRE, PD, RHU, SSD, EVI, LAI, Elevation |

### 2.4. Modeling and Validation

This study used SDMs to explore the suitable areas of stripe rust. Previous study has shown that there may be significant differences among different models, and it is difficult to determine any single model that consistently outperforms others in terms of prediction [41]. Moreover, ensemble models can eliminate the influence of poorly performing individual models, and their performance is generally slightly better than that of untuned individual models [42]. Therefore, in order to improve the stability of the model, we chose to use ensemble modeling methods. Modeling was performed in the R environment v4.1.2 using the BIOMOD2 package [43]. The BIOMOD2 package is a platform that can combine models to predict the distribution of species and test the relationship between species and the environment. It contains 10 single models, which can be run independently, or multiple models can be selected for ensemble modeling approach.

The algorithms used in this study to construct the ensemble model include three regression algorithms, two classification algorithms, three machine learning algorithms, and MaxEnt. The regression algorithms include a general linear model (GLM), general additive model (GAM), and multivariate adaptive regression splines (MARS) [44–46]. Classification methods include classification tree analysis (CTA) and flexible discriminant analysis (FDA) [47,48]. Machine learning methods include random forest (RF), an artificial neural network (ANN), and a generalized boosting model (GBM) [49–51]. MaxEnt has been widely applied due to its small data requirements, simple software operation, and relatively good results [52].

Building these models requires not only the presence data but also the pseudo-absences. We chose the "random" parameter to generate three sets of pseudo-absences because Barbet-Massin et al. [53] showed that the "random" method performed well in a variety of models and that random selection of pseudo-absences maximizes specificity, making the predicted distribution of a species only consist of the area where the species is highly likely to be present. The generated three sets of pseudo-absences were combined with the presences to form three sets of data, and 70% of each set was used as training data and the remaining 30% as test data. Thus, a total of three sets of training data and three sets of test data were utilized. Nine algorithms were used to train the three training sets three times, and a total of 81 models were obtained.

The performance of the model was evaluated by the area under the receiver operating characteristic curve (AUC) and true skills statistics (*TSS*). AUC and *TSS* are defined based on a confusion matrix (Table 3). *Sensitivity* and *specificity* are defined according to the confusion matrix, as shown in Formulas (2) and (3).

$$Sensitivity = \frac{a}{(a+b)} \tag{2}$$

$$Specificity = \frac{d}{(c+d)} \tag{3}$$

The receiver operating characteristic (ROC) curve is obtained by plotting all *sensitivity* values on the $y$-axis against their equivalent ($1 - specificity$) values for all available thresholds on the $x$-axis, and AUC is the area under the ROC curve [54]. AUC values range from 0.5 to 1. The AUC of a random model is 0.5, and the closer to 1, the better the model. *TSS* improves upon the kappa coefficient to remove its dependence on prevalence and retain all its advantages [55]. *TSS* is defined as:

$$TSS = Sensitivity + Specificity - 1 \tag{4}$$

The range of *TSS* values is from $-1$ to 1, where 1 means that the model is perfect, and less than or equal to 0 means the model performance is not better than random model.

**Table 3.** Confusion matrix for binary classification.

| Validation Data | Model | |
|---|---|---|
| | **Presence** | **Absence** |
| Presence | a | b |
| Absence | c | d |

The models with *TSS* > 0.8 were selected from the 81 models trained on monthly data, and the weighted average method was used to build an ensemble model, where the weight of each model was proportional to the *TSS* value [43].

We calculated the average value of the importance of each variable across all the models in the ensemble model, and the value of variable importance is between 0 and 1. The BIOMOD2 package uses a randomization procedure to estimate variable importance, and this process is not based on a specific model and can be compared across models. Specifically, this method calculates the correlation coefficient between the model prediction when the variable under investigation is randomly permuted in the initial model prediction. The higher the correlation, the lower the importance of the variable [56].

## 3. Results

### 3.1. Variable Importance

In this study, we used various types of data such as remote sensing, meteorology, biology, and plant protection to build monthly models. The variable importance ranges from 0 to 1, with 0 indicating that the variable has no effect on the model. In general, the importance of variables varied among the models, and meteorological factors were consistently the most important. The variables of importance results are shown in Figure 4.

Among the meteorological factors, temperature and precipitation are more important. From December to March, the importance of TMN is much greater than that of other variables, with the highest value in February reaching 0.59, followed by January, December, and March with values of 0.57, 0.55, and 0.43, respectively. The importance values of TMP in April to June are 0.20, 0.28, and 0.14, respectively. In July and August, the importance values of TMX are 0.22 and 0.08, respectively. PRE in summer (June–August) contributed the most to the model, with importance values of 0.45, 0.55, and 0.48, respectively. The importance values of PRE in other months ranged from 0.18 to 0.26. Other meteorological variables contributed significantly only in certain months. RHU ranks in the top three in the variable importance ranking in December, reaching 0.23. PD was in the top three in March with a value of 0.15. The impact of SSD in December and January was small, but the importance values of other months were all greater than 0.10, especially in May, which ranked first with an importance value of 0.39.

Elevation is an indispensable variable, second only to precipitation in importance in summer. The importance values for June, July, and August are 0.39, 0.35, and 0.29, respectively.

The importance of EVI has obvious seasonal characteristics. From December to March, the importance of EVI was relatively low, with a maximum of 0.07. However, the importance of EVI in April, May, and June were 0.43, 0.35, and 0.39, respectively, and decreased slightly in July and August to 0.31 and 0.23, respectively. The importance value of LAI ranged from 0.03 to 0.08 from December to July and reached the highest value of 0.21 in August.

### 3.2. Model Validation

Models were evaluated using AUC and TSS, where the AUC value is between 0.5 and 1, and the TSS value is between −1 and 1. Table 4 shows the TSS and AUC of ensemble models. The AUC values of the models ranged from 0.971 to 0.991, and the TSS values ranged from 0.851 to 0.931. August had the highest TSS and AUC values. The TSS in April was the lowest, and the AUC in June was the lowest. The average TSS and AUC values were calculated for the single algorithm model, and the results are shown in Table 5. The

RF model performed the best among single models, followed by MaxEnt and GLM, and CTA performed the worst. It can be seen that the performance of the ensemble model was improved compared with the single model.

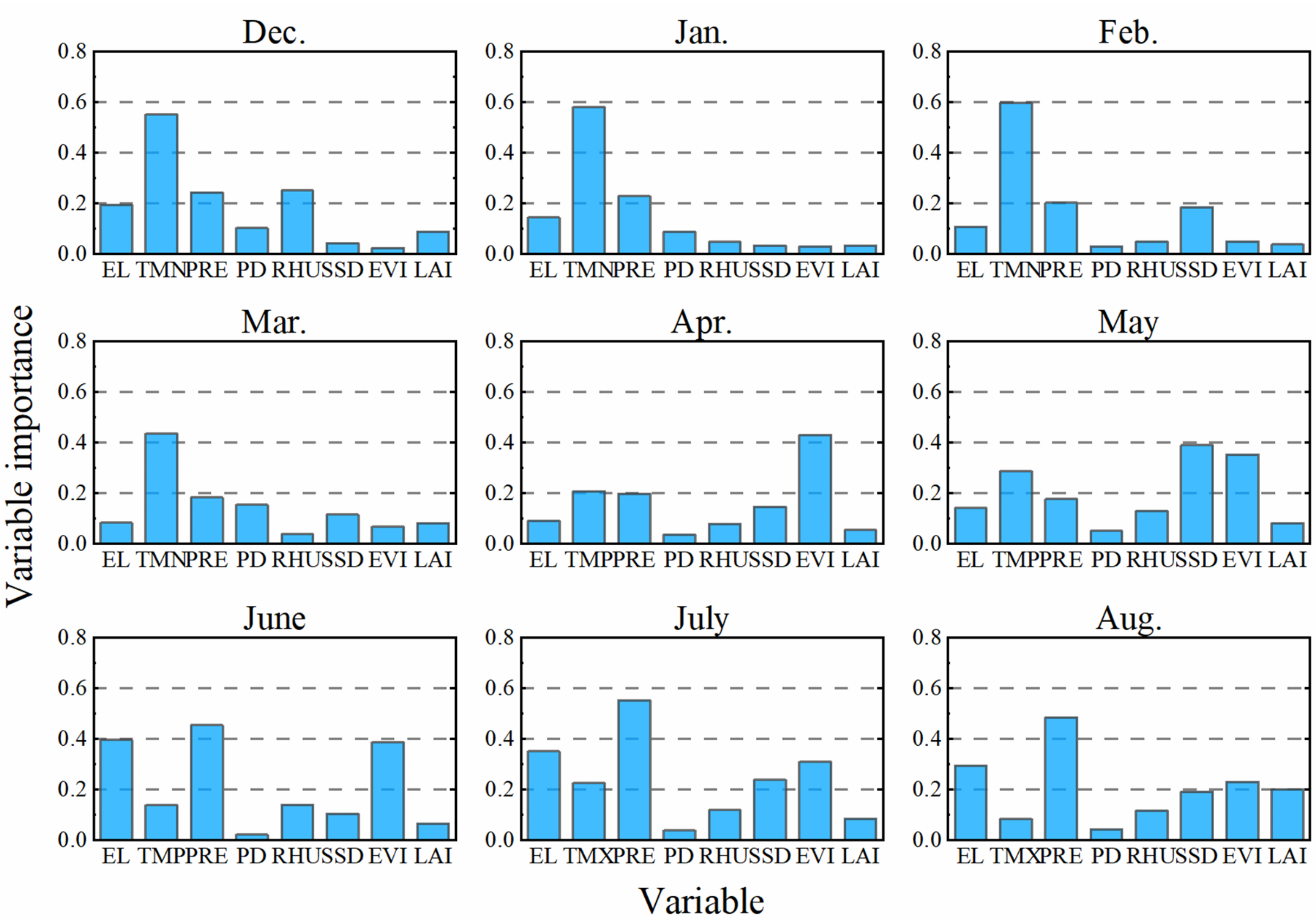


**Figure 4.** Variable importance of ensemble models from December to August.

### 3.3. Wheat Stripe Rust Suitable Areas

The suitable areas of stripe rust from December to August were simulated using monthly ensemble models (Figure 5). On the whole, stripe rust was distributed in the wheat-growing areas of northwest, southwest, Huang-Huai-Hai, and middle and lower reaches of the Yangtze River in China, mainly including Gansu, Shaanxi, Xinjiang, Chongqing, Sichuan, Guizhou, Yunnan, Hebei, Shandong, Henan, and Hubei.

**Table 4.** TSS and AUC of the ensemble models. The AUC value is between 0.5 and 1, while the TSS value is between −1 and 1.

| | December | January | February | March | April | May | June | July | August |
|---|---|---|---|---|---|---|---|---|---|
| TSS | 0.906 | 0.917 | 0.912 | 0.891 | 0.851 | 0.859 | 0.853 | 0.911 | 0.931 |
| AUC | 0.981 | 0.982 | 0.982 | 0.975 | 0.973 | 0.979 | 0.971 | 0.986 | 0.991 |

In December, wheat stripe rust was mainly distributed in winter wheat-growing areas in Southern and Eastern Gansu, the Guanzhong area in Shaanxi, Southern Sichuan and the Sichuan Basin, Western Guizhou, Yunnan, and Southwestern Xinjiang (Figure 5a). After that, it spread to the east, reaching wheat areas in Southern Henan, Northern Hubei, Chongqing, and Guizhou in February (Figure 5c).

**Table 5.** TSS and AUC of the single models. The AUC value is between 0.5 and 1, while the TSS value is between −1 and 1.

| | Model | December | January | February | March | April | May | June | July | August |
|---|---|---|---|---|---|---|---|---|---|---|
| TSS | ANN | 0.841 | 0.892 | 0.896 | 0.873 | 0.781 | 0.742 | 0.815 | 0.785 | 0.812 |
| | CTA | 0.825 | 0.839 | 0.871 | 0.842 | 0.776 | 0.736 | 0.782 | 0.831 | 0.824 |
| | FDA | 0.792 | 0.868 | 0.855 | 0.862 | 0.775 | 0.730 | 0.805 | 0.837 | 0.852 |
| | GAM | 0.836 | 0.891 | 0.872 | 0.877 | 0.802 | 0.737 | 0.821 | 0.823 | 0.847 |
| | GBM | 0.855 | 0.881 | 0.887 | 0.868 | 0.799 | 0.731 | 0.809 | 0.852 | 0.889 |
| | GLM | 0.865 | 0.899 | 0.898 | 0.873 | 0.812 | 0.777 | 0.822 | 0.879 | 0.867 |
| | MARS | 0.855 | 0.886 | 0.884 | 0.874 | 0.805 | 0.742 | 0.823 | 0.861 | 0.878 |
| | MAXENT | 0.863 | 0.889 | 0.877 | 0.879 | 0.804 | 0.753 | 0.837 | 0.890 | 0.892 |
| | RF | 0.900 | 0.909 | 0.907 | 0.889 | 0.843 | 0.788 | 0.849 | 0.900 | 0.927 |
| AUC | ANN | 0.943 | 0.964 | 0.972 | 0.956 | 0.938 | 0.915 | 0.940 | 0.919 | 0.936 |
| | CTA | 0.912 | 0.917 | 0.939 | 0.926 | 0.905 | 0.882 | 0.906 | 0.929 | 0.910 |
| | FDA | 0.941 | 0.965 | 0.966 | 0.961 | 0.944 | 0.919 | 0.950 | 0.955 | 0.963 |
| | GAM | 0.954 | 0.966 | 0.970 | 0.962 | 0.948 | 0.922 | 0.952 | 0.948 | 0.957 |
| | GBM | 0.964 | 0.968 | 0.972 | 0.959 | 0.949 | 0.915 | 0.953 | 0.966 | 0.977 |
| | GLM | 0.957 | 0.968 | 0.971 | 0.952 | 0.954 | 0.931 | 0.944 | 0.965 | 0.963 |
| | MARS | 0.958 | 0.967 | 0.965 | 0.960 | 0.948 | 0.923 | 0.950 | 0.960 | 0.973 |
| | MAXENT | 0.966 | 0.969 | 0.969 | 0.965 | 0.953 | 0.924 | 0.955 | 0.972 | 0.979 |
| | RF | 0.979 | 0.977 | 0.977 | 0.965 | 0.959 | 0.936 | 0.969 | 0.978 | 0.986 |

Compared with winter and summer, the suitable areas of stripe rust in spring were the widest. In March, wheat stripe rust was mainly distributed in Southwestern China, the Hanshui Basin, and Southern Henan wheat-growing areas (Figure 5d). Afterwards, stripe rust spread eastward to Henan, Anhui, and Jiangsu and northward to Shandong and Hebei wheat-growing areas. In April, winter wheat began to be harvested from south to north, and stripe rust continued to spread (Figure 5e). By May, stripe rust had become a widespread epidemic in the Guanzhong area, the middle and lower reaches of the Yangtze River, and the Huang-Huai-Hai wheat-planting areas (Figure 5f). The epidemic of stripe rust in northwestern wheat regions lagged behind other regions, and the development was slow in the early stage, but it began to spread rapidly after May.

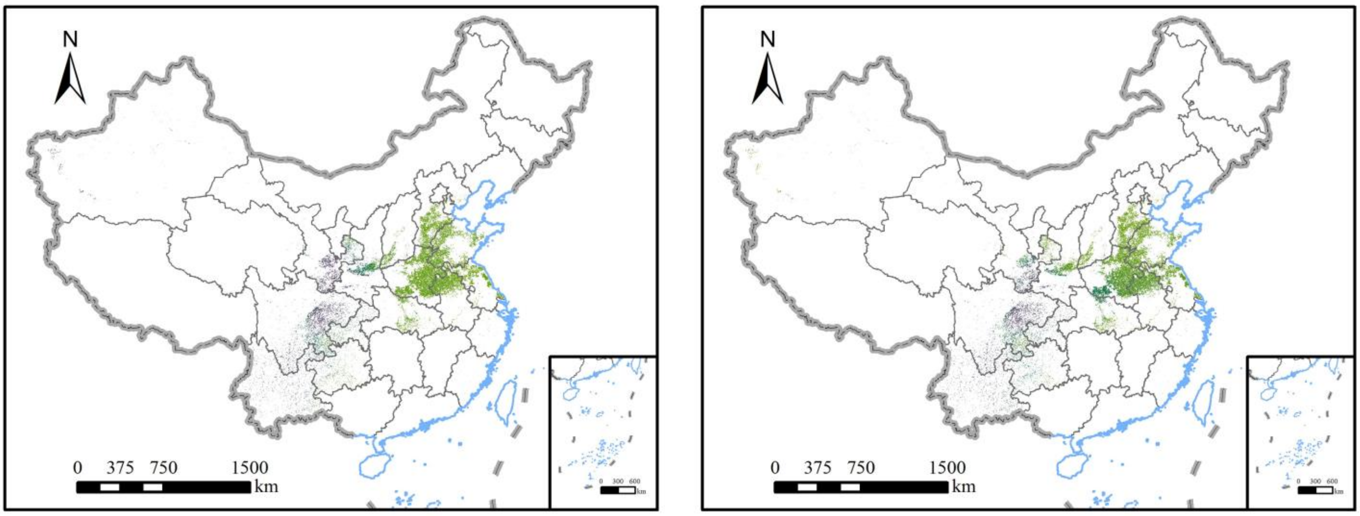


(**a**) December (**b**) January

**Figure 5.** *Cont.*

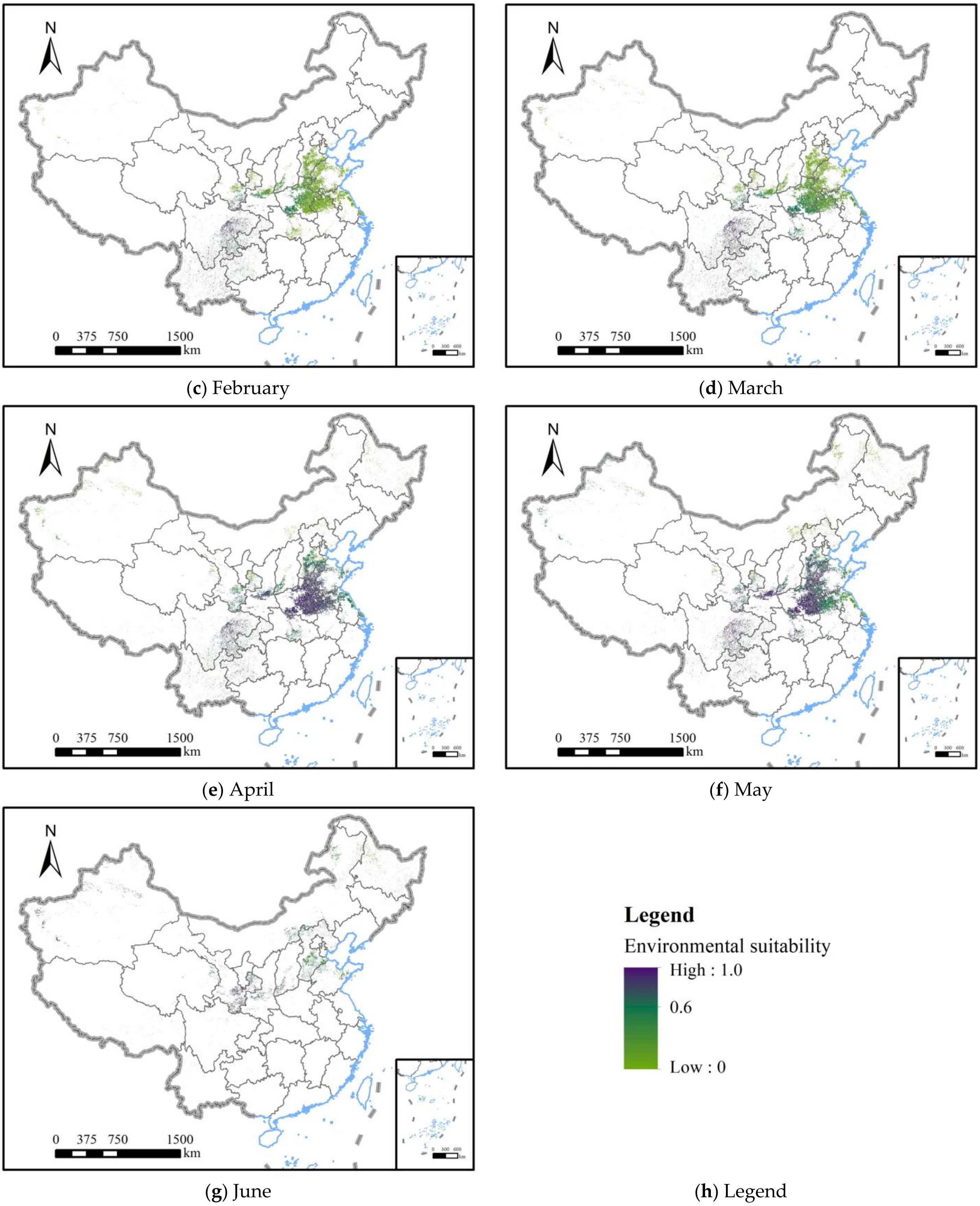


**Figure 5.** Environmental suitability of stripe rust from December to June in wheat-planting areas. (**a**) Environmental suitability of stripe rust in December of 2009–2013; (**b**–**g**): environmental suitability of stripe rust from January to June of 2010–2014, (**h**) Legend.

Most of the winter wheat had been harvested in June, and stripe rust was distributed on unripe wheat in Ulanqab City, Inner Mongolia, Southern and Eastern Gansu, Qinghai, Ningxia, Shaanxi, Shanxi, and Xinjiang (Figure 5g). After that, with the harvest of spring wheat, stripe rust occurred only on late-ripening spring wheat at higher elevation in Gansu, Ningxia, Qinghai, and Xinjiang.

### 3.4. Effects of Environmental Factors

Previous studies have divided the ecological zones of wheat stripe rust in China into 8 regions, as shown in Figure 6 [9]. In order to explore the impact of variables on the environmental suitability of wheat stripe rust in different regions, this study calculated the mean and standard deviation of each variable when the environmental suitability of wheat stripe rust was greater than 0.6 (high potential) in each region [57]. Figure 6 presents the results for each month for the five main regions.

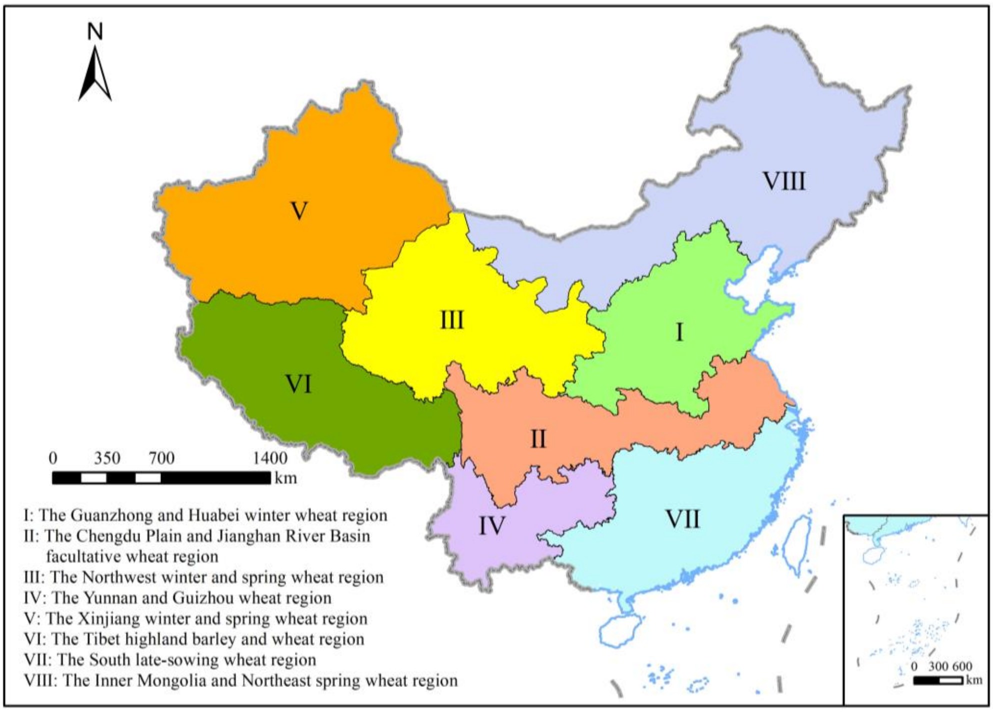


**Figure 6.** Wheat stripe rust ecological zones in China [9]. Adapted with permission from Ref. [9]. 2014, John Wiley and Sons.

The range of elevations suitable for stripe rust is very wide. Due to the higher terrain, the average elevations of stripe rust epidemic areas in Yunnan–Guizhou, the northwest, and Xinjiang are all above 1000 m, while those in Guanzhong, Huabei, the Chengdu Plain, and the Jianghan River Basin are lower. In terms of seasons, the suitable elevation of stripe rust in a single region in summer is higher than that in winter and spring. The suitable elevation for stripe rust in the northwest winter and spring wheat region has reached 2720 m, and the suitable elevation for wheat-planting areas in Guanzhong, Huabei, the Chengdu Plain and the Jianghan River Basin also increased significantly in summer because there are still some late-maturing wheats in these areas (Figure 7a).

Although different temperatures are used for different months in the modeling, the average temperature is used here for the convenience of unified comparison. The suitable average temperature in each region is in the range of −3.4 to 23.9 °C and is low in winter and high in summer. The suitable temperature in wheat-planting areas in the Chengdu Plain, the Jianghan River Basin, Guanzhong, Huabei, and Yunnan–Guizhou decreased slightly in summer, which is related to wheat harvesting in low-altitude areas (Figure 7b). The precipitation in winter is relatively low, and all regions are less than 50 mm. It starts to rise continuously in March in spring, reaching a maximum of 128 mm, and then fluctuates in summer (Figure 7c). The relative humidity is in the range of 50% to 80% in all regions except Xinjiang (Figure 7d). The suitable precipitation days for stripe rust are not less than 5 days in all regions (Figure 7e). Except for the Yunnan–Guizhou region, the average sunshine duration is lower in winter and higher in spring and summer, and the precipitation days are the opposite (Figure 7f).

In terms of vegetation variables, the variation of EVI values in different regions was different. The EVI of the Yunnan–Guizhou region is relatively stable over time, and the rest of the regions have certain changes over time. Among them, the larger the area of wheat planting, the greater the change of EVI, such as the Chengdu Plain, the Jianghan River Basin, and the Guanzhong and Huabei regions. The average value of EVI in these areas showed a clear trend of first rising and then falling with wheat growth and harvest (Figure 7g). LAI is relatively stable and low in winter, with an average value below 0.40. It started to increase in March in spring, and the changes in different regions were quite different after April (Figure 7h).

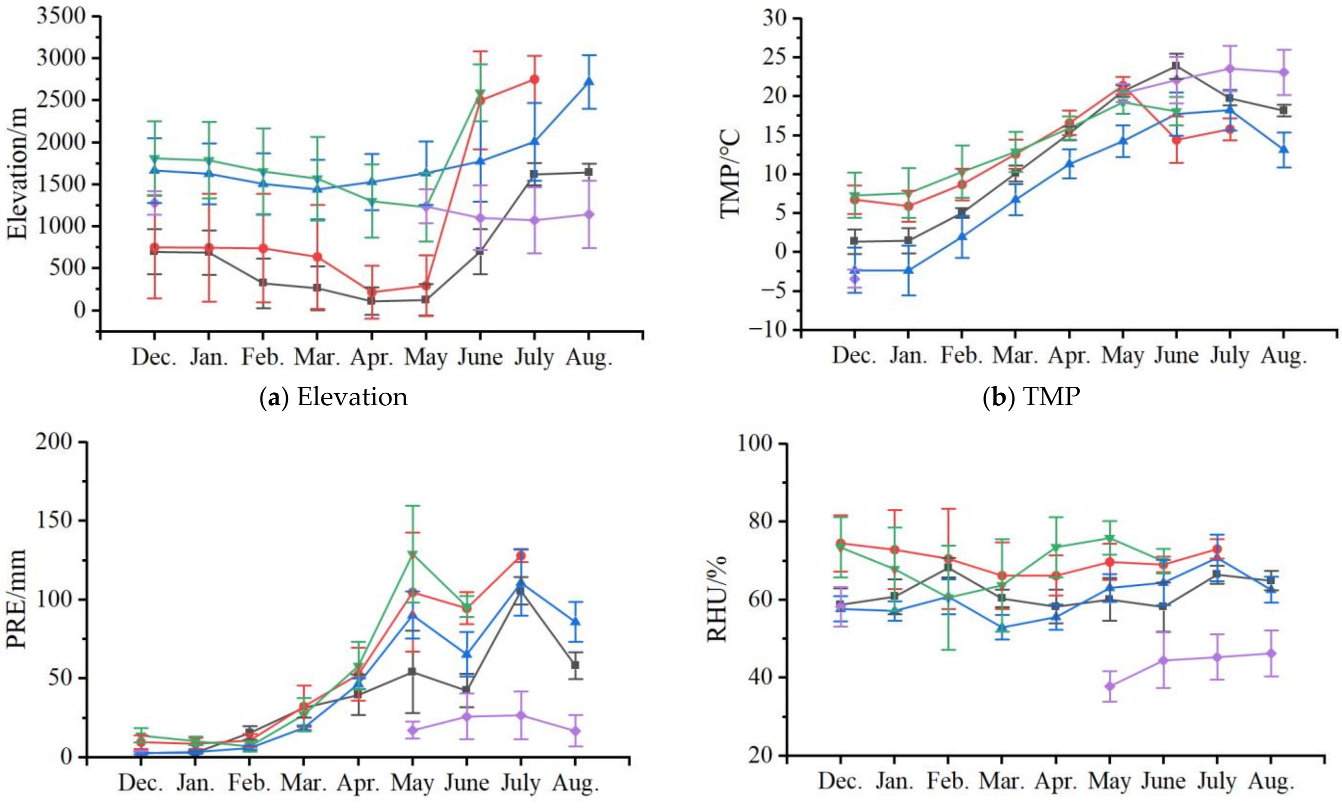


(**a**) Elevation (**b**) TMP

(**c**) PRE (**d**) RHU

**Figure 7.** *Cont.*

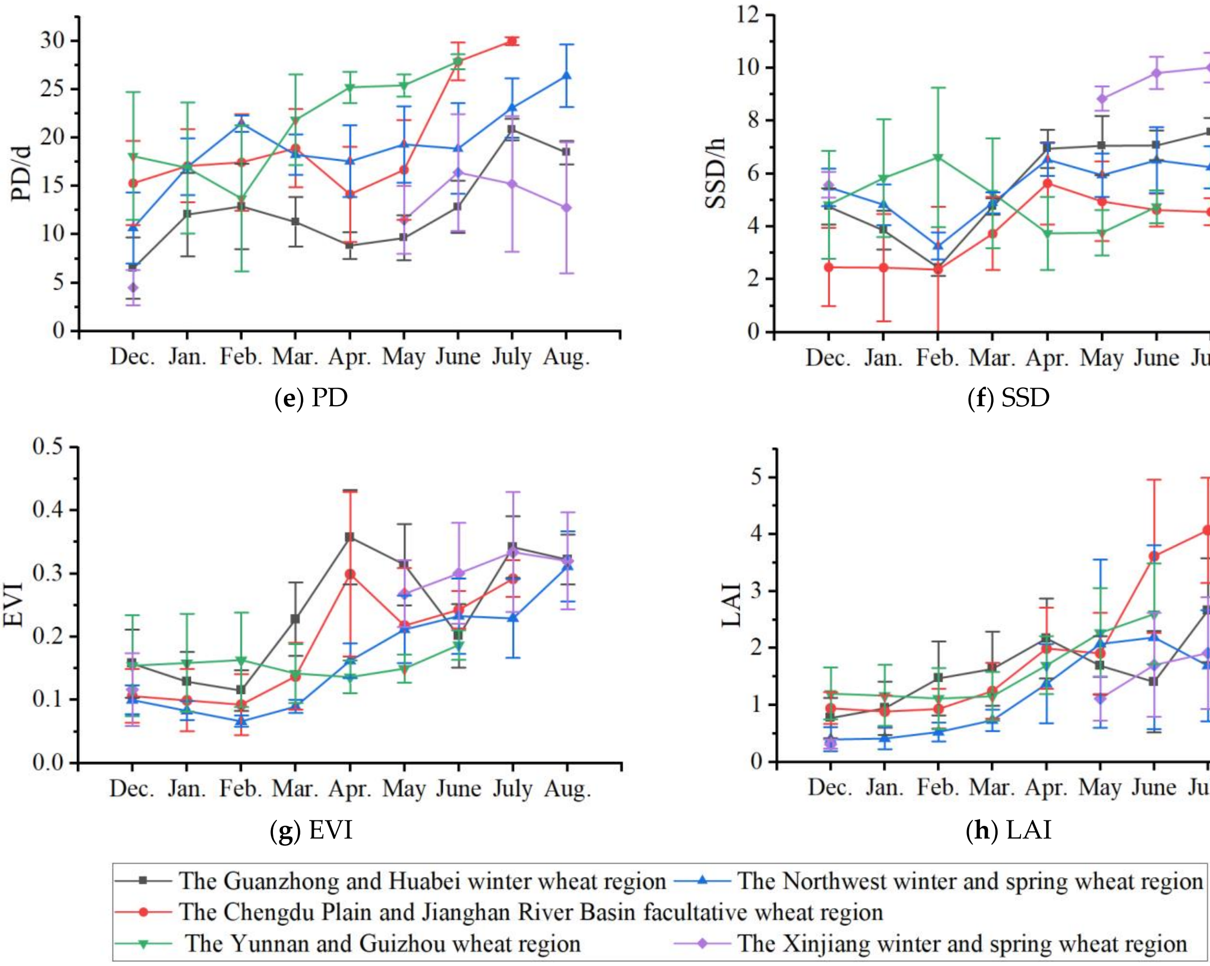


**Figure 7.** The mean and standard deviation of environmental variables in high-potential areas of major stripe rust ecological zones; (**a**–**h**) represent different environmental variables.

## 4. Discussion

This study used several types of variables to build the model. The results show that the epidemic of stripe rust is facilitated by a combination of factors, and various combinations of environmental factors can provide suitable living conditions for stripe rust.

Meteorological factors are the most important in modeling, with temperature and precipitation being the two most important. Temperature is most important in winter and early spring. Hu et al. built a temperature-based model for evaluating the overwintering potential of stripe rust using the temperature from 16 December to 15 March of the following year as the average temperature in winter and obtained satisfactory results [12]. Studies have shown that stripe rust can not only survive the winter but also multiply and spread in the Guanzhong Plain, dam areas, and plains of Sichuan and Yunnan, Hanzhong, and Ankang in Shaanxi, Xinyang in Henan, and Hubei [10,25]. Chen et al. believed that the stripe rust pathogen could infect host plants in the range of 0 to 23 °C, the optimum temperature was between 7 and 12 °C, and sporulation was faster at 15–25 °C [58]. In this study, the average temperature values of each region with environmental suitability greater than 0.6 are all in the first temperature range mentioned above except the northwest region and Xinjiang region in winter. Precipitation is always an important factor, especially in summer. High precipitation and high humidity in summer create favorable conditions for infection. Therefore, some studies suggested that stripe rust can be predicted by monitoring precipitation in a region and dew formation in fields [1].

The influence of elevation is great in winter and summer. Previous studies have shown that stripe rust has an upper elevation limit for overwintering regions such as Longnan and

Sichuan Aba and a lower elevation limit for oversummering regions such as the Northwest, Northwest Sichuan, and Yunnan–Guizhou [2]. Due to the spread of stripe rust to areas with lower elevations in the east in spring, the suitable elevations of stripe rust in the Chengdu Plain and Jianghan Valley wheat-planting areas, Guanzhong and Huabei wheat-planting areas, and Yunnan and Guizhou wheat-planting areas showed a downward trend before May [9,59]. After May, with the influence of factors such as the increase in temperature and wheat harvest in low-elevation areas, the suitable elevations in many areas increased significantly. Due to the huge difference in terrain, wheat was harvested early in plain and basin areas and late in high-elevation areas such as Aba, Ganzi, and Liangshan in Sichuan, so the changes in the average elevation of the Chengdu Plain and the Jianghan Basin are the most obvious [10,22].

Plants are mostly dormant in winter with no photosynthetic activity, and vegetation variables play a small role in the model [60]. The importance of EVI is greater after April because EVI can stably reflect vegetation conditions and wheat phenology [61]. This study shows that the vegetation variables when stripe rust is suitable are within a certain threshold range, which shows the importance of vegetation and its growth status to the occurrence and epidemic of stripe rust.

China has a large latitude and longitude span and complex terrain, which leads to large intra-regional climate differences. Therefore, not all regions are suitable for stripe rust occurrence and are largely limited by wheat-growing areas. The overwintering boundary of wheat stripe rust is generally considered to be along Huangling in Shaanxi Province, Jiexiu in Shanxi Province, Shijiazhuang in Hebei Province, and Dezhou of Shandong Province (latitude 37~38°N). Stripe rust can overwinter in the south of this boundary but generally cannot overwinter in the north [62]. The results obtained in this study were all within the above-mentioned overwintering regions. In the plains and dam areas of the Sichuan Basin, Northwestern Hubei, Southern Shaanxi, and Southern Henan with lower elevations. The temperature is relatively high, and the stripe rust pathogen can safely overwinter and even multiply and infect wheat seedlings [63]. In spring, stripe rust in overwintering region infects wheat plants and is transferred to the northeast by wind to the main winter wheat-planting areas [62,63]. At this time, in addition to the overwintering region, stripe rust was distributed in wheat-planting areas such as the Huang-Huai-Hai, the middle and lower reaches of the Yangtze River, and the Guanzhong Plain. The epidemic of stripe rust in northwestern wheat regions such as Xinjiang and Gansu lags behind other regions, and the development was slow in the early stage, but it began to spread rapidly after May [59]. With the harvest of wheat, stripe rust lost its main host plants in most areas and was mainly distributed in late-ripening spring wheat-planting areas in Gansu, Ningxia, Qinghai, and Xinjiang.

In fact, from the harvest of wheat to the emergence of autumn-sown winter wheat, volunteer wheat seedlings can serve as the host of stripe rust, transferring the pathogen from late-maturing winter and spring wheat to autumn-sown wheat seedlings, which plays a crucial role in the annual cycle of stripe rust [10,62]. Studies have shown that the northwest region, including Gansu, Eastern Qinghai, and Northwestern Sichuan, is the largest and most important oversummering region for stripe rust, in addition to the southwest (Yunnan, Guizhou), Xinjiang, and northern (Shanxi, Hebei) regions [11]. It can be seen that the estimation of the suitable areas of stripe rust in summer in this study is limited. In this study, disease occurrence data were collected during wheat planting, and overlap analysis was performed using published wheat-planting areas, which has also been performed in many previous studies for species with specific hosts [64,65]. However, due to the lack of data on the oversummering host of wheat stripe rust, this study focused on the risk of exposure to stripe rust during wheat planting, and the distribution results were smaller than the actual distribution of stripe rust. Therefore, in order to obtain the complete oversummering distribution of stripe rust, it is necessary to combine the alternate host plants. For example, Zhang et al. used overlapping analysis of the suitable planting areas of wheat, oversummering areas of stripe rust, and the richness of the simulated host (barberry) to predict the potential risk of wheat stripe rust in Sichuan under future conditions [7].

## 5. Conclusions

In the present study, data from various disciplinary fields such as remote sensing, meteorology, biology, and plant protection data were considered to study the suitable areas of stripe rust during wheat planting in China and emphasize the role of various variables in the occurrence of stripe rust in different periods. The accuracy results showed that the ensemble models performed better than the single models, with TSS and AUC greater than 0.851 and 0.971, respectively.

Among the three investigated types of environmental variables, meteorological variables contributed the most, with temperature and precipitation being the most important. Vegetation variables and elevation contributed significantly in some months. From the regional analysis of variables, although there are significant differences in the environment between different wheat producing areas, the combination of multiple environmental factors may still lead to the occurrence of stripe rust.

Due to the influence of climate, topography, and planting system, the distribution of the suitable areas for stripe rust varies at different times. In winter, stripe rust is mainly distributed in the Sichuan Basin, Northwestern Hubei, Southern Shaanxi, and Southern Henan wheat-planting areas. In spring, it spreads to the Huang-Huai-Hai and the middle and lower reaches of the Yangtze River and the Guanzhong Plain, and the development of stripe rust in the northwestern wheat-planting areas such as Xinjiang and Gansu lags behind. Wheat threatened by stripe rust is mainly distributed in late-ripening spring wheat-planting areas in Gansu, Ningxia, Qinghai, and Xinjiang in summer.

This study proved that it is possible to combine SDMs and multiple environmental variables to obtain the areas with environmental conditions suitable for stripe rust. However, limited by the data that could be collected, no host plants other than wheat were used in this study, which has certain limitations that should be considered in future studies. This study could provide new ideas and support for the prevention and control of wheat stripe rust.

**Author Contributions:** Conceptualization, Y.D., W.H. and X.C.; methodology, X.C. and L.H.; software, X.C.; validation, H.M. and H.Z.; formal analysis, Y.X. and J.W.; investigation, X.C. and H.M.; resources, H.Z.; data curation, X.C. and H.M.; writing—original draft preparation, X.C.; writing—review and editing, Y.D. and L.H.; visualization, Y.X. and J.W.; supervision, Y.D.; project administration, W.H.; funding acquisition, L.H., W.H. and Y.D. All authors have read and agreed to the published version of the manuscript.

**Funding:** This work was funded by National Key R&D Program of China (2021YFB3901300), National Natural Science Foundation of China (42071423, 32271986, 62273001), and Alliance of International Science Organizations (Grant No. ANSO-CR-KP-2021-06).

**Data Availability Statement:** All the data used in this study are available publicly. The ChinaCropPhen 1 km dataset is available from https://doi.org/10.6084/m9.figshare.8313530.v7 (accessed on 15 February 2022). The Digital Elevation Models are available from https://www.resdc.cn/data.aspx?DATAID=284 (accessed on 18 February 2022). The 1 km monthly minimum temperature dataset is available from https://doi.org/10.5281/zenodo.3114194 (accessed on 26 February 2022). The 1 km monthly mean temperature dataset is available from https://cstr.cn/18406.11.Meteoro.tpdc.270961 (accessed on 26 February 2022). The 1 km monthly maximum temperature dataset is available from https://doi.org/10.5281/zenodo.3114194 (accessed on 26 February 2022). The 1 km monthly precipitation dataset is available from https://doi.org/10.5281/zenodo.3185722 (accessed on 11 March 2022). The 1 km relative humidity dataset is available from https://doi.org/10.11866/db.loess.2018.245 (accessed on 18 March 2022). The 1 km sunshine duration dataset is available from https://doi.org/10.11866/db.loess.2018.173 (accessed on 24 February 2022). Global Land Surface Satellite (GLASS) product V60 is available from http://www.glass.umd.edu/Download.html (accessed on 3 April 2022). The ERA5-Land Hourly reanalysis dataset is available from https://cds.climate.copernicus.eu/cdsapp#!/dataset/reanalysis-era5-land?tab=overview (accessed on 13 April 2022). MOD09GA

V6.1 products are available from https://doi.org/10.5067/MODIS/MOD09GA.061 (accessed on 20 April 2022).

**Acknowledgments:** Data support from the National Earth System Science Data Center, National Science and Technology Infrastructure of China (http://www.geodata.cn), National Tibetan Plateau Data Center (http://data.tpdc.ac.cn), Resource and Environmental Science and Data Center, and Chinese Academy of Sciences (https://www.resdc.cn) is acknowledged. We are grateful to the academic editor and reviewers for their insightful comments, which greatly helped us improve the quality of this manuscript.

**Conflicts of Interest:** The authors declare no conflict of interest.

## References

1. Chen, X.M. Epidemiology and Control of Stripe Rust [*Puccinia Striiformis* f. Sp. *Tritici*] on Wheat. *Can. J. Plant Pathol.* **2005**, *27*, 314–337. [CrossRef]
2. Chen, W.Q.; Wu, L.R.; Liu, T.G.; Xu, S.C.; Jin, S.L.; Peng, Y.L.; Wang, B.T. Race Dynamics, Diversity, and Virulence Evolution in *Puccinia Striiformis* f. Sp. *Tritici*, the Causal Agent of Wheat Stripe Rust in China from 2003 to 2007. *Plant Dis.* **2009**, *93*, 1093–1101. [CrossRef]
3. Guisan, A.; Tingley, R.; Baumgartner, J.B.; Naujokaitis-Lewis, I.; Sutcliffe, P.R.; Tulloch, A.I.; Regan, T.J.; Brotons, L.; McDonald-Madden, E.; Mantyka-Pringle, C. Predicting Species Distributions for Conservation Decisions. *Ecol. Lett.* **2013**, *16*, 1424–1435. [CrossRef]
4. Lantschner, M.V.; de la Vega, G.; Corley, J.C. Predicting the Distribution of Harmful Species and Their Natural Enemies in Agricultural, Livestock and Forestry Systems: An Overview. *Int. J. Pest Manag.* **2019**, *65*, 190–206. [CrossRef]
5. Zhao, W.J.; Chen, L.; Ding, K.J. Prediction of potential geographic distribution areas of the maize downy mildew in China by using MAXENT. *Plant Prot.* **2009**, *35*, 32–38.
6. Cao, X.R.; Chen, L.; Zhou, Y.L. Potential distribution of Magnaporthe grisea in China and the world, predicted by MaxEnt. *Plant Prot.* **2011**, *37*, 80–83.
7. Zhang, N.N.; Liao, Z.Y.; Wu, S.; Nobis, M.P.; Wang, J.N.; Wu, N. Impact of Climate Change on Wheat Security through an Alternate Host of Stripe Rust. *Food Energy Secur.* **2022**, *11*, e356. [CrossRef]
8. Wellings, C.R. Global Status of Stripe Rust: A Review of Historical and Current Threats. *Euphytica* **2011**, *179*, 129–141. [CrossRef]
9. Chen, W.Q.; Wellings, C.; Chen, X.M.; Kang, Z.S.; Liu, T.G. Wheat Stripe (Yellow) Rust Caused by *Puccinia Striiformis* f. Sp. *Tritici*. *Mol. Plant Pathol.* **2014**, *15*, 433–446. [CrossRef]
10. Zeng, S.M.; Luo, Y. Long-Distance Spread and Interregional Epidemics of Wheat Stripe Rust in China. *Plant Dis.* **2006**, *90*, 980–988. [CrossRef]
11. Wan, A.M.; Chen, X.M.; He, Z.H. Wheat Stripe Rust in China. *Aust. J. Agric. Res.* **2007**, *58*, 605. [CrossRef]
12. Hu, X.; Cao, S.Q.; Cornelius, A.; Xu, X.M. Predicting Overwintering of Wheat Stripe Rust in Central and Northwestern China. *Plant Dis.* **2020**, *104*, 44–51. [CrossRef]
13. Bucchignani, E.; Montesarchio, M.; Cattaneo, L.; Manzi, M.P.; Mercogliano, P. Regional Climate Modeling over China with COSMO-CLM: Performance Assessment and Climate Projections. *J. Geophys. Res. Atmos.* **2014**, *119*, 12151–12170. [CrossRef]
14. Wang, C.C.; Li, L.F.; Jiang, B.B.; Zhang, K.Y.; Chu, B.Y.; Luo, Y.; Ma, Z.H. Genetic Diversity and Population Structure of *Puccinia Striiformis* f. Sp. *Tritici* Reveal Its Migration from Central to Eastern China. *Crop Prot.* **2020**, *128*, 104974. [CrossRef]
15. Coakley, S.M.; Line, R.F.; McDaniel, L.R. Predicting Stripe Rust Severity on Winter Wheat Using an Improved Method for Analyzing Meteorological and Rust Data. *Phytopathology* **1988**, *78*, 543–550. [CrossRef]
16. El Jarroudi, M.; Kouadio, L.; Bock, C.H.; El Jarroudi, M.; Junk, J.; Pasquali, M.; Maraite, H.; Delfosse, P. A Threshold-Based Weather Model for Predicting Stripe Rust Infection in Winter Wheat. *Plant Dis.* **2017**, *101*, 693–703. [CrossRef]
17. Vidal, T.; Boixel, A.; Maghrebi, E.; Perronne, R.; du Cheyron, P.; Enjalbert, J.; Leconte, M.; de Vallavieille-Pope, C. Success and Failure of Invasive Races of Plant Pathogens: The Case of *Puccinia Striiformis* f. Sp. *Tritici* in France. *Plant Pathol.* **2022**, *71*, 1525–1536. [CrossRef]
18. Sharma-Poudyal, D.; Chen, X.M. Models for Predicting Potential Yield Loss of Wheat Caused by Stripe Rust in the U.S. Pacific Northwest. *Phytopathology* **2011**, *101*, 544–554. [CrossRef] [PubMed]
19. Guo, X.; Wang, M.T.; Zhang, G.Z. Prediction model of meteorological grade of wheat stripe rust in winter-reproductive area, Sichuan Basin, China. *J. Appl. Ecol.* **2017**, *28*, 3994–4000. [CrossRef]
20. Naseri, B.; Sharifi, F. Predicting Wheat Stripe Rust Epidemics According to Influential Climatic Variables. *J. Plant Prot. Res.* **2019**, *59*, 519–528. [CrossRef]
21. Sandhu, S.K.; Dhaliwal, L.K.; Pannu, P.P.S. Effect of Weather Parameters on Incidence and Severity of Stripe Rust in Wheat under Natural and Artificial Conditions. *J. Agrometeorol.* **2017**, *19*, 272–277.
22. Wang, H.G.; Yang, X.B.; Ma, Z.H. Long-Distance Spore Transport of Wheat Stripe Rust Pathogen from Sichuan, Yunnan, and Guizhou in Southwestern China. *Plant Dis.* **2010**, *94*, 873–880. [CrossRef]
23. Sharma-Poudyal, D.; Chen, X.M.; Rupp, R.A. Potential Oversummering and Overwintering Regions for the Wheat Stripe Rust Pathogen in the Contiguous United States. *Int. J. Biometeorol.* **2014**, *58*, 987–997. [CrossRef] [PubMed]

24. Yang, X.D.; Nie, C.W.; Zhang, J.C.; Feng, H.K.; Yang, G.J. A Bayesian Network Model for Yellow Rust Forecasting in Winter Wheat. In *Proceedings of the Computer and Computing Technologies in Agriculture*; *XI*; Li, D.L., Zhao, C.J., Eds.; Springer International Publishing: Cham, Switzerland, 2019; Volume 545, pp. 65–75.
25. Wang, X.J.; Ma, Z.H.; Jiang, Y.Y.; Shi, S.D.; Liu, W.; Zeng, J.; Zhao, Z.W.; Wang, H.G. Modeling of the Overwintering Distribution of *Puccinia Striiformis* f. Sp. *Tritici* Based on Meteorological Data from 2001 to 2012 in China. *Front. Agric. Sci. Eng.* **2014**, *1*, 223. [CrossRef]
26. He, K.; Bradley, B.; Cord, A.; Rocchini, D.; Tuanmu, M.-N.; Schmidtlein, S.; Turner, W.; Wegmann, M.; Pettorelli, N. Will Remote Sensing Shape the next Generation of Species Distribution Models? *Remote Sens. Ecol. Conserv.* **2015**, *1*, 4–18. [CrossRef]
27. Austin, M.P.; Van Niel, K.P. Improving Species Distribution Models for Climate Change Studies: Variable Selection and Scale: Species Distribution Models for Climate Change Studies. *J. Biogeogr.* **2011**, *38*, 1–8. [CrossRef]
28. Leitão, P.J.; Santos, M.J. Improving Models of Species Ecological Niches: A Remote Sensing Overview. *Front. Ecol. Evol.* **2019**, *7*, 9. [CrossRef]
29. Qin, D.; Tao, S.; Dong, S.; Luo, Y. Climate, Environmental, and Socioeconomic Characteristics of China. In *Climate and Environmental Change in China: 1951–2012*; Springer Environmental Science and Engineering; Qin, D., Ding, Y., Mu, M., Eds.; Springer: Berlin/Heidelberg, Germany, 2016; pp. 1–27, ISBN 978-3-662-48482-1.
30. Wang, F.H.; He, Z.H.; Sayre, K.; Li, S.D.; Si, J.S.; Feng, B.; Kong, L. Wheat Cropping Systems and Technologies in China. *Field Crops Res.* **2009**, *111*, 181–188. [CrossRef]
31. Brown, J.L. SDMtoolbox: A Python-Based GIS Toolkit for Landscape Genetic, Biogeographic and Species Distribution Model Analyses. *Methods Ecol. Evol.* **2014**, *5*, 694–700. [CrossRef]
32. Luo, Y.C.; Zhang, Z.; Chen, Y.; Li, Z.Y.; Tao, F.L. ChinaCropPhen1km: A High-Resolution Crop Phenological Dataset for Three Staple Crops in China during 2000–2019 Based on LAI Products. In *Earth System Science Data Discussions*; Beijing Normal University: Beijing, China, 2021; p. 8621165535.
33. Tao, F.L.; Zhang, S.; Zhang, Z. Spatiotemporal Changes of Wheat Phenology in China under the Effects of Temperature, Day Length and Cultivar Thermal Characteristics. *Eur. J. Agron.* **2012**, *43*, 201–212. [CrossRef]
34. Peng, S.; Ding, Y.; Liu, W.; Li, Z. 1 Km Monthly Temperature and Precipitation Dataset for China from 1901 to 2017. *Earth Syst. Sci. Data* **2019**, *11*, 1931–1946. [CrossRef]
35. Sun, W.; Mu, X.; Song, X.; Wu, D.; Cheng, A.; Qiu, B. Changes in Extreme Temperature and Precipitation Events in the Loess Plateau (China) during 1960–2013 under Global Warming. *Atmos. Res.* **2016**, *168*, 33–48. [CrossRef]
36. Liang, S.; Cheng, J.; Jia, K.; Jiang, B.; Liu, Q.; Xiao, Z.; Yao, Y.; Yuan, W.; Zhang, X.; Zhao, X. The Global Land Surface Satellite (GLASS) Product Suite. *Bull. Am. Meteorol. Soc.* **2021**, *102*, E323–E337. [CrossRef]
37. Muñoz Sabater, J. ERA5-Land Hourly Data from 1981 to Present. *Copernic. Clim. Chang. Serv. C3S Clim. Data Store CDS* **2019**, *10*.
38. Vermote, E.; Wolfe, R. *MODIS/Terra Surface Reflectance Daily L2G Global 1km and 500m SIN Grid V061*; NASA EOSDIS Land Process. DAAC; LP DAAC: Sioux Falls, South Dakota, 2021; Volume 10. [CrossRef]
39. Hällfors, M.H.; Liao, J.; Dzurisin, J.; Grundel, R.; Hyvärinen, M.; Towle, K.; Wu, G.C.; Hellmann, J.J. Addressing Potential Local Adaptation in Species Distribution Models: Implications for Conservation under Climate Change. *Ecol. Appl.* **2016**, *26*, 1154–1169. [CrossRef]
40. Gilani, H.; Arif Goheer, M.; Ahmad, H.; Hussain, K. Under Predicted Climate Change: Distribution and Ecological Niche Modelling of Six Native Tree Species in Gilgit-Baltistan, Pakistan. *Ecol. Indic.* **2020**, *111*, 106049. [CrossRef]
41. Norberg, A.; Abrego, N.; Blanchet, F.G.; Adler, F.R.; Anderson, B.J.; Anttila, J.; Araújo, M.B.; Dallas, T.; Dunson, D.; Elith, J. A Comprehensive Evaluation of Predictive Performance of 33 Species Distribution Models at Species and Community Levels. *Ecol. Monogr.* **2019**, *89*, e01370. [CrossRef]
42. Hao, T.X.; Elith, J.; Lahoz-Monfort, J.J.; Guillera-Arroita, G. Testing Whether Ensemble Modelling Is Advantageous for Maximising Predictive Performance of Species Distribution Models. *Ecography* **2020**, *43*, 549–558. [CrossRef]
43. Thuiller, W.; Georges, D.; Engler, R.; Breiner, F.; Georges, M.D.; Thuiller, C.W. *Package 'Biomod2'—Species Distribution Modelling Ensemble Framework*; R Core Team: Vienna, Austria, 2016.
44. McCullagh, P. Generalized Linear Models. *Eur. J. Oper. Res.* **1984**, *16*, 285–292. [CrossRef]
45. Hastie, T.J. Generalized Additive Models. In *Statistical Models in S*; Routledge: New York, NY, USA, 1992; ISBN 978-0-203-73853-5.
46. Friedman, J.H. Multivariate Adaptive Regression Splines. *Ann. Stat.* **1991**, *19*, 1–67. [CrossRef]
47. Breiman, L. *Classification and Regression Trees*; Routledge: New York, NY, USA, 2017; ISBN 978-1-315-13947-0.
48. Hastie, T.; Tibshirani, R.; Buja, A. Flexible Discriminant Analysis by Optimal Scoring. *J. Am. Stat. Assoc.* **1994**, *89*, 1255–1270. [CrossRef]
49. Breiman, L. Random Forests. *Mach. Learn.* **2001**, *45*, 5–32. [CrossRef]
50. Ripley, B.D. *Pattern Recognition and Neural Networks*; Cambridge University Press: Cambridge, MA, USA, 2007.
51. Elith, J.; Leathwick, J.R.; Hastie, T. A Working Guide to Boosted Regression Trees. *J. Anim. Ecol.* **2008**, *77*, 802–813. [CrossRef] [PubMed]
52. Phillips, S.J.; Anderson, R.P.; Schapire, R.E. Maximum Entropy Modeling of Species Geographic Distributions. *Ecol. Model.* **2006**, *190*, 231–259. [CrossRef]
53. Barbet-Massin, M.; Jiguet, F.; Albert, C.H.; Thuiller, W. Selecting Pseudo-Absences for Species Distribution Models: How, Where and How Many? *Methods Ecol. Evol.* **2012**, *3*, 327–338. [CrossRef]

54. Fielding, A.H.; Bell, J.F. A Review of Methods for the Assessment of Prediction Errors in Conservation Presence/Absence Models. *Environ. Conserv.* **1997**, *24*, 38–49. [CrossRef]
55. Allouche, O.; Tsoar, A.; Kadmon, R. Assessing the Accuracy of Species Distribution Models: Prevalence, Kappa and the True Skill Statistic (TSS). *J. Appl. Ecol.* **2006**, *43*, 1223–1232. [CrossRef]
56. Thuiller, W.; Lafourcade, B.; Engler, R.; Araújo, M.B. BIOMOD—A Platform for Ensemble Forecasting of Species Distributions. *Ecography* **2009**, *32*, 369–373. [CrossRef]
57. Convertino, M.; Muñoz-Carpena, R.; Chu-Agor, M.L.; Kiker, G.A.; Linkov, I. Untangling Drivers of Species Distributions: Global Sensitivity and Uncertainty Analyses of MaxEnt. *Environ. Model. Softw.* **2014**, *51*, 296–309. [CrossRef]
58. Chen, X. Pathogens Which Threaten Food Security: Puccinia Striiformis, the Wheat Stripe Rust Pathogen. *Food Secur.* **2020**, *12*, 239–251. [CrossRef]
59. Wang, H.; Yang, X.; Ma, Z. Investigation of the Long-Distance Transports of *Puccinia Striiformis* f. Sp. *Tritici* in China Using HYSPLIT-4 Model. *J. China Agric. Univ.* **2010**, *15*, 55–64.
60. Wang, Z.; Schaaf, C.B.; Strahler, A.H.; Chopping, M.J.; Román, M.O.; Shuai, Y.; Woodcock, C.E.; Hollinger, D.Y.; Fitzjarrald, D.R. Evaluation of MODIS Albedo Product (MCD43A) over Grassland, Agriculture and Forest Surface Types during Dormant and Snow-Covered Periods. *Remote Sens. Environ.* **2014**, *140*, 60–77. [CrossRef]
61. Yan, F.; Shi, P.J.; Wu, J.J.; Wang, Y.J. Study on Phenology Character of Winter Wheat by Modis-Evi Data in Hebei China. In Proceedings of the IGARSS 2008-2008 IEEE International Geoscience and Remote Sensing Symposium, Boston, MA, USA, 6–11 July 2008; Volume 1, pp. I-327–I-330.
62. Zeng, Q.D.; Zhao, J.; Wu, J.H.; Zhan, G.M.; Han, D.J.; Kang, Z.S. Wheat Stripe Rust and Integration of Sustainable Control Strategies in China. *Front. Agric. Sci. Eng.* **2022**, *9*, 37–51. [CrossRef]
63. Zeng, Q.-D.; Han, D.-J.; Wang, Q.-L.; Yuan, F.-P.; Wu, J.-H.; Zhang, L.; Wang, X.-J.; Huang, L.-L.; Chen, X.-M.; Kang, Z.-S. Stripe Rust Resistance and Genes in Chinese Wheat Cultivars and Breeding Lines. *Euphytica* **2014**, *196*, 271–284. [CrossRef]
64. Kriticos, D.J.; Morin, L.; Leriche, A.; Anderson, R.C.; Caley, P. Combining a Climatic Niche Model of an Invasive Fungus with Its Host Species Distributions to Identify Risks to Natural Assets: Puccinia Psidii Sensu Lato in Australia. *PLoS ONE* **2013**, *8*, e64479. [CrossRef]
65. da Cunha, H.F.; Ferreira, É.D.; Tessarolo, G.; Nabout, J.C. Host Plant Distributions and Climate Interact to Affect the Predicted Geographic Distribution of a Neotropical Termite. *Biotropica* **2018**, *50*, 625–632. [CrossRef]